doi:10.1093/brain/awaa383 BRAIN 2021: 144; 266–277 | 266

BRAIN
A JOURNAL OF NEUROLOGY

^{18}F-AV-1451 positron emission tomography in neuropathological substrates of corticobasal syndrome

Anna E. Goodheart,[1,2] Joseph J. Locascio,[1,2] Wesley R. Samore,[3] Jessica A. Collins,[1,4] Michael Brickhouse,[1,4] Aaron Schultz,[2,4,5] Alexandra Touroutoglou,[1,4] Keith A. Johnson,[1,2,4,5] Matthew P. Frosch,[2,3] John H. Growdon,[1,2] Bradford C. Dickerson[1,2,4] and Stephen N. Gomperts[1,2]

Multiple neuropathological processes can manifest in life as a corticobasal syndrome. We sought to relate retention of the tau-PET tracer ^{18}F-AV-1451 and structural magnetic resonance measures of regional atrophy to clinical features in clinically diagnosed and neuropathologically confirmed cases of corticobasal syndrome and to determine whether these vary with the underlying neuropathological changes. In this observational, cross-sectional study, 11 subjects (eight female and three male, median age 72 years) with corticobasal syndrome underwent structural MRI, tau-PET with ^{18}F-AV-1451, amyloid-PET with ^{11}C-Pittsburgh compound B, detailed clinical examinations and neuropsychological testing. Of the 11, three had evidence of high amyloid burden consistent with Alzheimer's disease while eight did not. Neuropathological evaluations were acquired in six cases. Mixed effects general linear models were used to compare ^{18}F-AV-1451 retention and atrophy in amyloid-negative corticobasal syndrome cases to 32 age-matched healthy control subjects and to relate cortical and subcortical ^{18}F-AV-1451 retention and atrophy to clinical features. Subjects without amyloid, including three with pathologically confirmed corticobasal degeneration, showed greater regional ^{18}F-AV-1451 retention and associated regional atrophy in areas commonly associated with corticobasal degeneration pathology than healthy control subjects [retention was higher compared to healthy controls ($P = 0.0011$), driven especially by the precentral gyrus ($P = 0.011$) and pallidum ($P < 0.0001$), and greater atrophy was seen in subjects compared to control subjects ($P = 0.0004$)]. Both ^{18}F-AV-1451 retention and atrophy were greater in the clinically more affected hemisphere [on average, retention was 0.173 standardized uptake value ratio units higher on the more affected side (95% confidence interval, CI 0.11–0.24, $P < 0.0001$), and volume was 0.719 lower on the more affected side (95% CI 0.35–1.08, $P = 0.0001$)]. ^{18}F-AV-1451 retention was greater in subcortical than in cortical regions, $P < 0.0001$. In contrast to these findings, subjects with amyloid-positive corticobasal syndrome, including two neuropathologically confirmed cases of Alzheimer's disease, demonstrated greater and more widespread ^{18}F-AV-1451 retention and regional atrophy than observed in the amyloid-negative cases. There was thalamic ^{18}F-AV-1451 retention but minimal cortical and basal ganglia uptake in a single corticobasal syndrome subject without neuropathological evidence of tau pathology, likely representing non-specific signal. Asymmetric cortical and basal ganglia ^{18}F-AV-1451 retention consonant with the clinical manifestations characterize corticobasal syndrome due to corticobasal degeneration, whereas the cortical retention in cases associated with Alzheimer's disease is greater and more diffuse.

1 Department of Neurology, Massachusetts General Hospital, Charlestown, MA, USA
2 Massachusetts Alzheimer's Disease Research Center, Massachusetts General Hospital, Boston, MA, USA
3 Department of Pathology, Massachusetts General Hospital, Boston, MA, USA
4 Athinoula A. Martinos Center for Biomedical Imaging, Massachusetts General Hospital, Charlestown, MA, USA
5 Department of Radiology, Massachusetts General Hospital, Boston, MA, USA

Received March 20, 2020. Revised August 18, 2020. Accepted August 24, 2020. Advance access publication November 22, 2020

Correspondence to: Stephen N. Gomperts, MD, PhD
Department of Neurology
Building 114, 16th Street - 2004
Charlestown, MA 02129-4404, USA
E-mail: gomperts.stephen@mgh.harvard.edu

Keywords: corticobasal degeneration; corticobasal syndrome; AV-1451; tau-PET

Abbreviations: AN-CBS = amyloid-negative corticobasal syndrome; CBD = corticobasal degeneration; CBS = corticobasal syndrome; PiB = Pittsburgh compound B; PSP = progressive supranuclear palsy; PVC = partial volume correction; SUVR = standardized uptake value ratio

Introduction

Initially described by Rebeiz *et al.* (1967), corticobasal degeneration (CBD) is defined neuropathologically by neuronal and glial tau inclusions with a topography that includes the basal ganglia and cortex (Dickson *et al.*, 2002; Arnold *et al.*, 2013). CBD is difficult to diagnose in life, due to poor one-to-one correlation between clinical phenotype and underlying CBD pathology. Only approximately 24–54% of patients presenting with corticobasal syndrome (CBS), characterized clinically by progressive asymmetric cortical and extrapyramidal motor deficits as well as variable cognitive and behavioural symptoms (Armstrong *et al.*, 2013), have been found to harbour neuropathological changes of CBD (Boeve *et al.*, 1999; Ling *et al.*, 2010; Lee *et al.*, 2011). In the remainder of cases, other pathologies have been explanatory, foremost among them Alzheimer's disease (Boeve *et al.*, 1999; Ling *et al.*, 2010; Lee *et al.*, 2011; Jabbari *et al.*, 2019). To contend with this clinical-pathological discordance, there is a pressing need for imaging tools that can differentiate the neurodegenerative diseases underlying CBS in life, both to aid in diagnosis and to enable treatment trials.

Although asymmetric atrophy and associated cortical and subcortical hypometabolism in CBS permit its differentiation from other clinical syndromes (Upadhyay *et al.*, 2016; Niccolini *et al.*, 2018; Walker *et al.*, 2018), these features do not distinguish the underlying neuropathological causes of CBS. In principle, molecular imaging with PET tracers targeting the neuropathological aggregates of tau that accumulate in CBD would provide a powerful tool for this purpose.

Several PET tracers have been developed to image tau species (Villemagne *et al.*, 2015). The most widely used of these is ^{18}F-AV-1451 (also known as flortaucipir) (Chien *et al.*, 2013; Xia *et al.*, 2013). Based on its high affinity for paired helical filaments (PHF) of 3-repeat and 4-repeat (3R/4R) tau present in the Alzheimer's disease brain, ^{18}F-AV-1451 has enabled successful antemortem tau imaging in Alzheimer's disease (Johnson *et al.*, 2016), in combination with amyloid-PET (Klunk *et al.*, 2004). ^{18}F-AV-1451 has also been under increasing study in patients with CBS (Josephs *et al.*, 2016; McMillan *et al.*, 2016; Cho *et al.*, 2017; Smith *et al.*, 2017; Xia *et al.*, 2017; Ali *et al.*, 2018; Coakeley *et al.*, 2018; Niccolini *et al.*, 2018; Tsai *et al.*, 2019). Although ^{18}F-AV-1451 has not demonstrated robust *in vitro* binding to tau aggregates in CBD, which are composed primarily of 4-repeat (4R) straight filaments (Marquie *et al.*, 2015; Lowe *et al.*, 2016; Sander *et al.*, 2016; Ono *et al.*, 2017), several studies have shown subtle but significant ^{18}F-AV-1451 retention in brain areas susceptible to CBD tau pathology in patients with CBS (Josephs *et al.*, 2016; McMillan *et al.*, 2016; Cho *et al.*, 2017; Smith *et al.*, 2017; Xia *et al.*, 2017; Niccolini *et al.*, 2018), perhaps due to small amounts of PHF tau in neuronal inclusions (Tatsumi *et al.*, 2014). While the reported magnitude of ^{18}F-AV-1451 retention in CBS patients has been low compared to the high retention observed in Alzheimer's disease, the neuropathologically appropriate spatial topography of tracer retention has raised the possibility that ^{18}F-AV-1451 may have clinical utility in patients with CBS.

To evaluate the potential clinical significance of ^{18}F-AV-1451 retention in CBS, we investigated *in vivo* images in a series of 11 subjects diagnosed with CBS. Six of these patients underwent autopsy, and three were found to have CBD, two had Alzheimer's disease, and one had non-specific pathology without evidence for tauopathy. Using amyloid PET to exclude CBS cases due to Alzheimer's disease, we also compared amyloid-negative CBS (AN-CBS) subjects presumably enriched for CBD with normal control subjects to relate clinical features to regional ^{18}F-AV-1451 retention and to structural magnetic resonance-based measures of regional atrophy. We hypothesized that ^{18}F-AV-1451 retention would be asymmetrically increased and clinically predictive in both the neuropathologically proven cases of CBD and the cases of AN-CBS and would be minimal in the CBS case lacking tau pathology, contrasting with marked uptake in the amyloid-positive cases attributable to Alzheimer's disease. We further hypothesized that in CBD and AN-CBS, the hemisphere with greater retention would predict the clinically more affected side and that these results would be mirrored by asymmetric atrophy.

Materials and methods

Participant selection and clinical assessments

This study was approved by the Partners Healthcare Institutional Review Board. Subjects or subjects' surrogates provided informed consent to participate in the study. Eleven

subjects between the ages of 50 and 85 years were recruited based on availability from the Massachusetts General Hospital (MGH) Memory Disorders Unit, Frontotemporal Disorders Unit, or Movement Disorders Unit. Participants were diagnosed using consensus diagnostic criteria for CBS (Armstrong *et al.*, 2013). Exclusion criteria included major psychiatric comorbidities, use of cognition-impairing medications, and a history of stroke or other significant structural brain lesions. Because of the intentionally low specificity of the lowest level of diagnostic certainty of the Hoglinger criteria for the clinical diagnosis of progressive supranuclear palsy ('suggestive of PSP'), all but one subject met criteria for this category (Hoglinger *et al.*, 2017). The remaining subject met Hoglinger criteria for possible PSP (PSP with predominant CBS). Subjects were kept on their antiparkinsonian medications throughout the study, as applicable, and were required to be on stable doses of medications with CNS effects for at least 3 months prior to the study. Subjects underwent a full medical history, physical examination, and detailed neurological examination, including Unified Parkinson's Disease Rating Scale (UPDRS) (Goetz *et al.*, 2008) by a neurologist experienced in movement disorders. Detailed neuropsychological testing was obtained, with tests selected from the Uniform Data Set of the Alzheimer's Disease Centers (Weintraub *et al.*, 2009) to evaluate the following cognitive domains: executive function, visuospatial skills, language, and episodic memory. Neuropsychological test scores were compared to normalized data from cognitively normal subjects taken from the Massachusetts Alzheimer's Disease Research Center database to generate *z*-scores for each cognitive domain. A *z*-score $\leqslant -1.5$ was considered impaired. Imaging data from 32 age-matched cognitively normal subjects recruited for an independent study at MGH were used as imaging controls (NIH grant R01 AG046396, K.J.).

Neuroimaging procedures and processing

^{18}F-AV-1451 and ^{11}C-Pittsburgh compound B (^{11}C-PiB) ligands were prepared and administered at MGH, as previously described (Mathis *et al.*, 2003; Shoup *et al.*, 2013; Johnson *et al.*, 2016). PET data were acquired using a Siemens/CTI, ECAT HR + scanner (3D mode; 63 image planes; 15.2 cm axial field of view; 5.6 mm transaxial resolution and 2.4 mm slice interval). ^{18}F-AV-1451-PET was acquired from 80–100 min after a 9–11 mCi bolus injection. ^{11}C-PiB-PET was acquired with an 8.5–15 mCi bolus injection followed immediately by a 60-min dynamic acquisition. Magnetic resonance scans were acquired using a Siemens 3 T Tim Trio system to generate high-resolution magnetization prepared rapid gradient echo (MP-RAGE) images. Cortical thickness and subcortical deep grey volumes were calculated using FreeSurfer (http://surfer.nmr.mgh.harvard.edu) surface-based and volume-based pipelines (Fischl and Dale, 2000; Fischl *et al.*, 2004) and compared to normalized MRIs to generate atrophy *z*-scores, as has been previously described (Bakkour *et al.*, 2009; Dickerson *et al.*, 2009). PET data were reconstructed, corrected for attenuation, and co-registered to MP-RAGE sequences and were spatially normalized to a template brain using statistical parametric mapping (SPM8, Wellcome Department of Cognitive Neurology, London). For ^{18}F-AV-1451-PET, standardized uptake value ratios (SUVRs) were computed using a cerebellar grey matter reference region, with and without partial volume correction (PVC) using FreeSurfer's symmetric geometric transfer matrix (SGTM) (Greve *et al.*, 2016). For ^{11}C-PiB-PET, distribution volume ratios (DVRs) were computed with the cerebellar grey as reference, using the Logan graphical method (Logan *et al.*, 1996). PiB DVRs in the frontal-lateral temporal-retrosplenial aggregate $\geqslant 1.2$ were considered amyloid-positive (Johnson *et al.*, 2016). A region of interest-based approach was chosen for MRI and ^{18}F-AV-1451-PET analyses, focused on brain areas known to harbour significant tau pathology in CBD (Dickson *et al.*, 2002), resulting in eight bilateral regions of interest for each subject, comprising four cortical regions (superior frontal, superior parietal, precentral, postcentral) and four subcortical regions (caudate, putamen, pallidum, thalamus).

Neuropathology

Autopsies were performed according to standardized protocols (Vonsattel *et al.*, 2008) at the Massachusetts Alzheimer's Disease Research Center. At the time of autopsy, brains were divided at the midline, with one hemisphere sectioned and frozen at –80°C and the other fixed in 10% buffered formalin. After 10 to 14 days, the formalin-fixed hemisphere was sectioned, photographed, and evaluated grossly by a board-certified neuropathologist. In each case, 25 tissue sections were obtained utilizing a blocking protocol that widely samples anatomical regions relevant for diagnosis of neurodegenerative disorders. These regions included the hippocampus, thalamus, subthalamic nucleus, basal ganglia, amygdala, cerebellum with dentate nucleus, and all levels of the brainstem. Multiple sections of frontal, parietal, temporal, cingulate, and calcarine cortices were also sampled. The tissue blocks were processed on a Thermo Scientific Excelsior ES tissue processor, and embedded in paraffin. All sections were cut on a microtome at 7 μmol/l and stained with Luxol fast blue/haematoxylin and eosin for routine assessment. Bielschowsky silver stain was carried out on sections from select blocks. Immunohistochemistry was performed on sections from select blocks and processed on a Leica Bond RX automated stainer (Leica Biosystems), with anti-human pan-tau antibody (Dako), anti-human beta-amyloid antibody (Dako), anti-GFAP antibody (Sigma-Aldrich), anti-TDP-43 antibody (Proteintech), and anti-synuclein antibody (Thermo Scientific), as well as anti-ubiquitin antibody in the case of Subject 11 (ThermoFisher). Neuropathological examination was performed in accordance with published guidelines (Cairns *et al.*, 2007; Hyman *et al.*, 2012). All subjects who underwent autopsy were retrospectively assessed for histological burden of tau deposition utilizing the pan-tau antibody. Key anatomical regions were evaluated independently for tau deposition due to CBD or due to Alzheimer's disease using a semi-quantitative scale. Those regions with no tau positivity were assessed as '0'. When present, the degree of CBD-related tau deposition was graded on a 1 to 3 scale, with a score of '1' indicating sparse CBD-related tau inclusions of any kind (e.g. the glial and neuronal inclusions seen in CBD), with many microscopic fields devoid of inclusions. A score of '2' correlated to moderate numbers of inclusions (some but not all microscopic fields containing inclusions), and '3' correlated to a frequent, heavy burden of inclusions (such that every microscopic field contained inclusions). When present, the degree of Alzheimer's disease-related tau deposition was independently graded on a 1 to 3 scale, with a score of '1' indicating sparse Alzheimer's disease-

related tau inclusions of any kind (e.g. the neurofibrillary tangles, dystrophic neurites, and neuritic plaques seen in Alzheimer disease), '2' correlated to moderate numbers of inclusions, and '3' correlated to a frequent, heavy burden of inclusions (Mirra *et al.*, 1991). CBD neuropathological diagnosis was based on the Office of Rare Diseases neuropathological criteria (Dickson *et al.*, 2002). Alzheimer's disease neuropathological changes were scored according to the National Institute on Aging-Alzheimer's Association guidelines (Hyman *et al.*, 2012).

Statistical analysis

^{11}C-PiB-PET and neuropathology, when available, were used to stratify CBS subjects into an amyloid-positive group associated with Alzheimer's disease ($n = 3$), a tau-negative amyloid-negative (non-CBD, non-Alzheimer's disease) subject ($n = 1$), a neuropathologically-proven CBD group ($n = 3$), and a group of amyloid-negative CBS subjects presumed to harbour CBD pathology but without neuropathological confirmation ($n = 4$). The latter two groups were combined into an amyloid-negative CBS ('AN-CBS') group ($n = 7$) for group-level analyses with normal control subjects. The asymmetry of tau-PET retention, measured as the absolute value of the left-right difference in ^{18}F-AV-1451 SUVR (separately for PVC and non-PVC data), was compared across diagnostic groups (AN-CBS versus normal controls) for each of the eight regions of interest using a mixed between (diagnosis) and within (region of interest) subject factorial ANOVA, which included a Diagnosis × Region of interest interaction term. Adjusted Tukey *post hoc* tests were used to identify regions of interest in which asymmetry differed between the diagnostic groups. The asymmetry of regional atrophy, measured as the absolute value of the left-right difference in magnetic resonance atrophy *z*-scores, was compared across diagnostic groups for each of the regions of interest using the same approach. Residuals from these models were examined graphically for conformance to the assumptions of normality and homoscedasticity.

Tau-PET retention (^{18}F-AV-1451 SUVRs) and regional atrophy (magnetic resonance atrophy *z*-scores) were compared across diagnostic groups (AN-CBS versus normal controls) and the clinically affected side (for AN-CBS subjects only) using mixed effects general linear models. In each analysis, the dependent variable was tau-PET uptake or regional atrophy. The individual data record was a unilateral region of interest for each of the eight regions of interest for each subject. Based on clinical motor evaluation, one side was considered dysfunctionally affected and the other less so, in the case of AN-CBS subjects, and one side was left and the other right in the case of normal control subjects. For AN-CBS subjects, regions of interest were classified as being in the predominantly affected hemisphere (contralateral to the side of more severe motor symptoms) or in the less affected hemisphere (ipsilateral to the side of more severe motor symptoms); for normal control subjects, both left and right hemispheres were used. The fixed effect predictors in the model were the categorical variables of diagnostic group (AN-CBS or normal controls, a subject-level variable), side affected, and region of interest, as well as the interaction of Diagnostic group × Region of interest and of Side affected × Region of interest. The random effect term was subjects nested within diagnostic group. A backward elimination algorithm was applied to the fixed and random effects in the full model. Adjusted Tukey *post hoc* tests were applied to any significant overall effects involving regions of interest to pinpoint the locus of overall effect. Residuals from the fixed and random predicted values were examined graphically for conformance to the assumptions of normality and homoscedasticity. Follow-up analyses were run on the tau-PET data that were structurally identical to those detailed above but which included a major region factor (cortical or subcortical) as a fixed effect. Individual regions of interest were modelled as a nested factor within their respective major region. Statistical significance was defined as an adjusted P-value < 0.05. SAS version 9.4 and JMP Pro version 14.0 were used for analyses and graphing.

Data availability

These data are available from the corresponding author upon reasonable request.

Results

Subjects

Demographics, clinical features, results of neuropsychological testing, amyloid status, and neuropathological findings at autopsy (when available) of the 11 CBS cases and normal control subjects are shown in Table 1 and Supplementary Table 1. All CBS subjects had markedly asymmetric extrapyramidal impairments, including hemiparkinsonism and/or hemidystonia and met consensus diagnostic criteria for CBS (Armstrong *et al.*, 2013). One subject (Subject 7) had cortical sensory loss, apraxia, hemidystonia, and hemiparkinsonism but also had slightly reduced upgaze and downgaze amplitude and reduced vertical saccade speed; his clinical features did not fulfil clinical diagnostic criteria for PSP-Richardson syndrome but met criteria for possible PSP (PSP with predominant CBS) (Hoglinger *et al.*, 2017). Vertical gaze was normal in the remaining subjects. On neuropsychological testing, executive dysfunction was universal. Additional language, visuospatial, and memory impairments were common. Eight participants (Subjects 1–7 and 11) (Table 1) were amyloid-negative as defined by ^{11}C-PiB DVR <1.2 (median 1.005, range 0.926–1.147). The age of the 11 CBS subjects (median 72, range 52–81 years) and the age of the 32 normal control subjects (median 70, range 45–88 years) were similar ($P = 0.4$, Student's two-tailed *t*-test).

Tau-PET imaging of distinct neuropathologies presenting as CBS

In neuropathologically confirmed CBD, asymmetrically elevated ^{18}F-AV-1451 retention in cortex and basal ganglia paralleled the deposition of tau. Figure 1A shows ^{18}F-AV-1451 PET and MRI in such a case: a 60-year-old male (Subject 2) with left-sided hemiparkinsonism, left-sided cortical sensory deficits, bilateral apraxia, and executive and language dysfunction. MRI was notable for right > left frontal and parietal atrophy. Focal, asymmetric, and moderate ^{18}F-AV-1451 retention was evident in the right

Table 1 Demographics and features of CBS subjects

	Subject 1	Subject 2	Subject 3	Subject 4	Subject 5	Subject 6	Subject 7	Subject 8	Subject 9	Subject 10	Subject 11
Demographics											
Sex	Male	Male	Female	Female	Female	Female	Male	Female	Female	Female	Female
Age	56	60	72	72	74	81	72	52	61	75	59
Education	16	16	14	18	20	16	18	18	16	12	16
Handedness	Right	Right	Right	Right	Right	Right	Left	Right	Right	Right	Right
Motor											
Side affected	Right	Left	Left	Left	Left	Right	Right	Left	Left	Left	Left
UPDRS	Unknown	13	74	16	56	18	31	17	24	24	18
Cognitive											
MMSE	7	29	21	20 (MoCA)	23	25	23	21	26	27	22
CDR-SOB	10	0	1.5	1.5	1.5	0.5	3	4	3	0.5	5.5
Domains	E, V, L, M	E, L	E, L[a]	E, V, M	E, L	E, V	E, V, L, M	E, V, L	E, M	E	E
Diagnostics											
PiB DVR	0.93 (–)	1.04 (–)	1.15 (–)	0.99 (–)	1.01 (–)	1.00 (–)	0.99 (–)	CSF+	1.78 (+)	1.62 (+)	1.03 (–)
Path	CBD	CBD	CBD, AD	–	–	–	–	AD	AD	–	Other
PET-path interval	1.6	3.8	1.9	–	–	–	–	3.4	5.3	–	2.8

Age reported is age at time of ^{18}F-AV-1451 scan. Education is reported in years. Side affected refers to the side with the greatest motor impairments on neurological exam. UPDRS = Unified Parkinson's Disease Rating Scale, motor subscale (Goetz *et al.*, 2007). Subject 1 was too cognitively impaired at the time of neurological exam to reliably participate in UPDRS testing. MMSE = Mini-Mental State Examination; MoCA = Montreal Cognitive Assessment (Subject 4 had a MoCA instead of MMSE) (Folstein *et al.*, 1975; Nasreddine *et al.*, 2005); CDR-SOB = Clinical Dementia Rating Scale Sum of Boxes score (Morris, 1997). Domains refers to impaired cognitive domains on neuropsychological testing (Weintraub *et al.*, 2009), defined as a z-score $\leqslant -1.5$ on one or more tests of that domain (E = executive; L = language; M = memory; V = visuospatial). PiB DVR = ^{11}C PiB distribution volume ratio; amyloid positivity was determined using a threshold of DVR $\geqslant$ 1.2. Subject 8 was unable to tolerate PiB-PET and instead underwent CSF testing for amyloid-β_{42} (261.8 pg/ml), total tau (647.9 pg/ml), and phospho-tau [93.8 pg/ml (diagnostic cut-off $>$ 61.0 pg/ml)], with amyloid-tau index of 0.26 (diagnostic cut-off $<$ 1.0); the results were consistent with Alzheimer's disease. 'Path' refers to neuropathological diagnosis, when available. AD = Alzheimer's disease. For Subject 11, 'Other' refers to isolated thalamic gliosis. 'PET-path interval' refers to years between ^{18}F-AV-1451 scan and autopsy. Demographics of the 32 cognitively normal control subjects were as follows: age, median 70 years, range 45–88 years; gender, 16 females and 16 males; education, median 16 years, range 12–20 years; MMSE, median 30, range 28–30.

[a]Subject 3 declined to complete the full neuropsychological testing battery.

precentral gyrus (primary motor cortex) and bilateral basal ganglia (right > left). The focal cortical retention of ^{18}F-AV-1451 colocalized with focal cortical atrophy (Supplementary Fig. 1A). Neuropathology confirmed CBD as the diagnosis, with moderate numbers of tau-positive inclusions in cortical neurons and scattered ballooned cells on Luxol fast blue/haematoxylin and eosin (Supplementary Table 1). Many astrocytic plaques were present, particularly in the motor cortex, which had the greatest burden of cortical tau pathology compared with other cortical regions. Mild-to-moderate numbers of oligodendroglial inclusions (coiled bodies) were seen within the white matter of the cerebral hemispheres, with the greatest number present in the white matter underlying the motor cortex. Scattered tufted astrocytes and moderate numbers of tau-positive threads involving both grey and white matter were also present. A similar distribution and morphology of tau inclusions were observed in the two additional cases of neuropathologically confirmed CBD (Supplementary Table 1). In all cases, PiB-PET was negative for amyloid. Although Subject 3 had a subthreshold PiB DVR (1.147), cortical and basal ganglia ^{18}F-AV-1451 retention was more diffuse than in the other CBD cases (Supplementary Fig. 2). By the time of autopsy 2 years later, both CBD and moderate Alzheimer's disease co-pathology (A2B2C2, Braak tangle stage III) were present (Braak and Braak, 1991; Hyman *et al.*, 2012).

In contrast to the focal, clinically meaningful, but relatively low magnitude ^{18}F-AV-1451 retention pattern in isolated CBD, high magnitude ^{18}F-AV-1451 retention characterized CBS due to neuropathologically confirmed Alzheimer's disease. Figure 1B shows ^{18}F-AV-1451 PET and MRI in such a case: a 52-year-old female (Subject 8) who presented with left upper extremity myoclonus and apraxia, left alien limb phenomenon, left > right cortical sensory loss, as well as executive, visuospatial, and language dysfunction. MRI was notable for diffuse but asymmetric (right > left) cortical atrophy. Cortical ^{18}F-AV-1451 retention was markedly elevated in the Alzheimer's disease range and was widely distributed asymmetrically across the cortex (right > left). Neuropathological evaluation was notable for severe Alzheimer's disease pathological changes, with a heavy burden of neuritic plaques and neurofibrillary tangles (A3B3C3, Braak tangle stage VI), as well as concomitant Lewy body disease, corresponding to Braak stage 4. Similar neuroimaging results were observed in the two additional CBS cases with positive Alzheimer's disease biomarkers (Supplementary Fig. 3). Subject 9, the other amyloid-positive subject to undergo autopsy, was also found to have severe Alzheimer's disease pathological changes (A3B3C3, Braak tangle stage VI) (Supplementary Table 1).

A CBS subject without neuropathological evidence of tau pathology provided an informative contrast to the pathologically proven cases harbouring tau. Figure 1C shows ^{18}F-AV-1451 PET and MRI acquired in a 59-year-old female (Subject 11) who presented with left > right rigidity, left-sided cortical sensory loss, and executive dysfunction. In

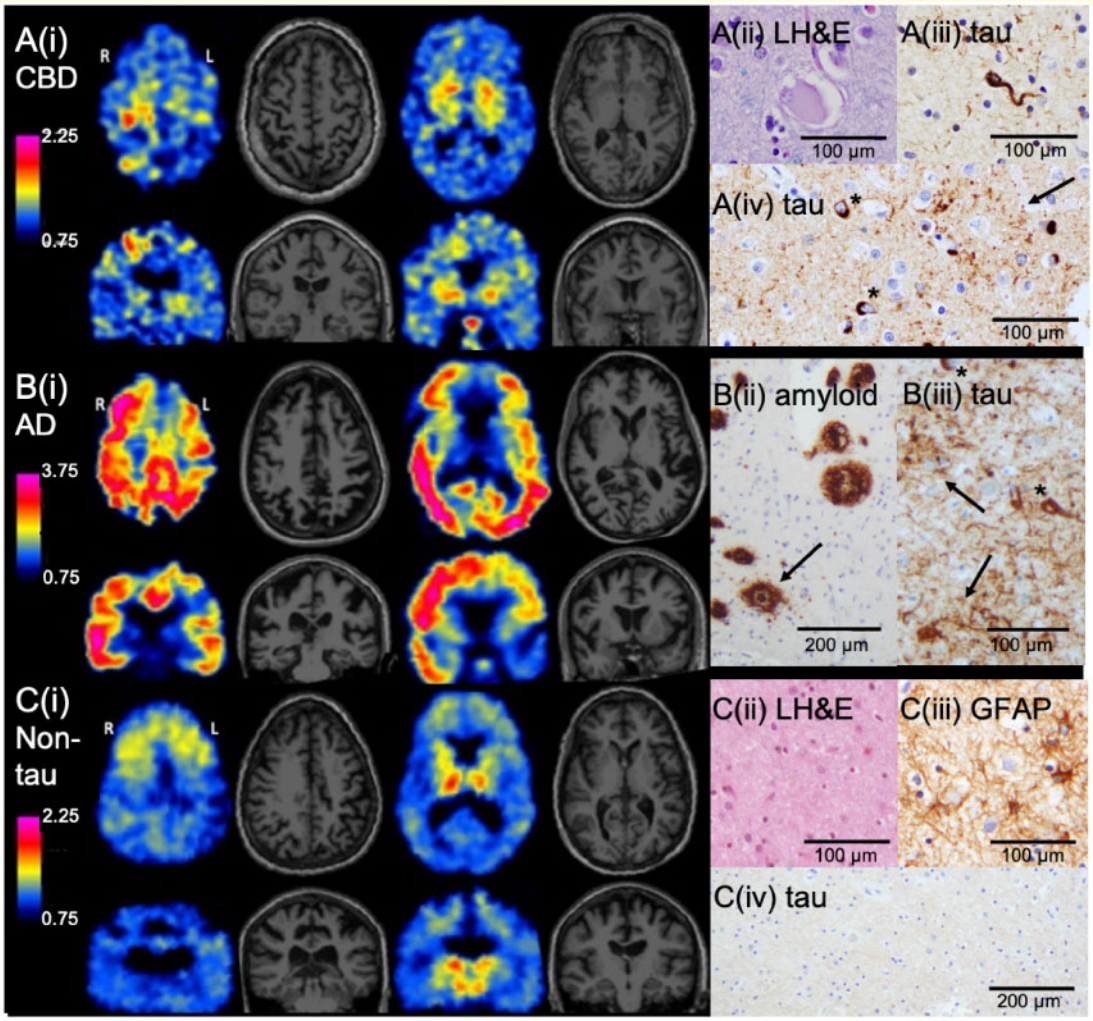

Figure 1 Representative axial and coronal slices of ^{18}F-AV-1451 PET and MRI and associated neuropathological findings in three cases of CBS. (**A**) CBS subject (aged 60 years) with left-predominant motor symptoms and neuropathologically confirmed CBD (Subject 2). [**A**(**i**)] ^{18}F-AV-1451 retention was most notable in the right precentral gyrus and bilateral basal ganglia. Off-target binding was present in the pituitary. Neuropathological analyses confirmed CBD. [**A**(**ii**)] Rare ballooned cortical neurons were present in frontal cortex. [**A**(**iii**)] A moderate burden of tau-positive coiled bodies (oligodendrocyte cytoplasmic inclusions) was present in underlying white matter. [**A**(**iv**)] The burden of cortical tau pathology was greatest in the right precentral gyrus (shown), compared with the parietal, occipital, and temporal lobes. Immunohistochemistry with anti-tau antibody demonstrated numerous astrocytic plaques (arrow) and intraneuronal inclusions (asterisks). (**B**) CBS subject (aged 52 years) with left predominant motor symptoms and neuropathologically confirmed Alzheimer's disease (AD) (Subject 8). [**B**(**i**)] Widespread but asymmetric cortical ^{18}F-AV-1451 retention was present. Note the modified colour scale, with higher upper value, to capture the high levels of tracer retention present in this Alzheimer's disease case. [**B**(**ii**)] Immunohistochemistry with anti-amyloid-β antibody demonstrated a heavy burden of dense-cored (arrow) and diffuse plaques. Parietal cortex is shown. [**B**(**iii**)] Anti-tau antibody in parietal cortex showed numerous neuritic plaques (arrows) and neurofibrillary tangles (asterisks). (**C**) CBS subject (aged 59 years) with left predominant motor symptoms without evidence for tau pathology on neuropathological assessment (Subject 11). [**C**(**i**)] ^{18}F-AV-1451 retention was evident in the bilateral thalami and the bilateral substantia nigra, and to a lesser extent symmetrically in the frontal subcortical and perithalamic white matter and the basal ganglia. [**C**(**ii**)] Neuropathology demonstrated prominent gliosis with neuronal dropout in the thalamus, including in the dorsomedian nucleus (shown). [**C**(**iii**)] Immunohistochemistry with anti-GFAP antibody showed numerous reactive astrocytes in the thalamus. [**C**(**iv**)] Immunohistochemistry with anti-tau antibody in the thalamus (shown) and other regions was negative for abnormal tau accumulation. ^{18}F-AV-1451 SUVR scales are shown for each subject. GFAP = glial fibrillary acidic protein; LH&E = Luxol fast blue/haematoxylin and eosin.

contrast to the frontal and parietal cortical atrophy present in this case, cortical ^{18}F-AV-1451 retention was minimal. Instead, elevated ^{18}F-AV-1451 retention was present in the bilateral thalami, right > left, and to a lesser degree in the perithalamic and frontal subcortical white matter and basal ganglia. In contrast to the CBD case, in this case of CBS without tau pathology, regional cortical atrophy did not colocalize with cortical retention of ^{18}F-AV-1451 (Supplementary Fig. 1C). Off-target binding in the substantia nigra was observed, as previously reported (Marquie *et al.*,

2015; Lowe *et al.*, 2016; Sander *et al.*, 2016; Ono *et al.*, 2017). On neuropathological assessment, the thalamic retention of ^{18}F-AV-1451 corresponded with thalamic gliosis (Supplementary Table 1). Immunohistochemistry was negative for tau, as well as for amyloid, TDP-43, and α-synuclein. Immunohistochemistry for ubiquitin was negative for neuronal inclusions within the thalamus, frontal cortex, temporal cortex, and parietal cortex. Additional assessments, including analysis of tissue at the National Prion Disease Pathology Surveillance Center, were negative for prion pathology. Antemortem genetic testing was also negative for alterations in *C9orf72*, *GRN*, and *MAPT*. The pattern of ^{18}F-AV-1451 retention in this tau-negative case—with high thalamic retention and symmetric and modest basal ganglia and frontal subcortical white matter retention, and with discordant focal cortical atrophy and ^{18}F-AV-1451 cortical retention—contrasts with both the pattern of asymmetric focal cortical grey matter and basal ganglia retention seen in the CBD and AN-CBS cases, and with the pattern of elevated and diffuse cortical retention seen in the cases with positive Alzheimer's disease biomarkers.

Correlation of tau-PET imaging with clinical features

Consistent with the asymmetric clinical features of both the neuropathologically proven CBD cases and the AN-CBS participants (Subjects 1–7) more broadly, ^{18}F-AV-1451 retention was asymmetric in both basal ganglia and cortical motor regions (Fig. 1A). To quantify the extent of the asymmetry, we used mixed-between and within-subject factorial ANOVAs for ^{18}F-AV-1451 retention in AN-CBS and normal control subjects (see 'Materials and methods' section). These analyses identified a significant interaction between region of interest and diagnostic group (each $P < 0.0001$), with greater asymmetry overall in AN-CBS (main effect of diagnosis, $P < 0.0001$). *Post hoc* tests showed that in the precentral gyrus, superior parietal gyrus, thalamus, and pallidum, the extent of the asymmetry of ^{18}F-AV-1451 retention was significantly greater in AN-CBS than in normal control subjects (for each region of interest, Tukey-adjusted $P \leqslant 0.05$), whereas the difference was not significant or only marginally so in the other regions of interest.

To confirm that the retention pattern of ^{18}F-AV-1451 in these amyloid-negative putative CBD cases was clinically meaningful and reflected asymmetric motor features, we used mixed effects general linear models (see 'Materials and methods' section). In these analyses, a main effect of higher ^{18}F-AV-1451 retention in AN-CBS subjects' more clinically affected side than in the less affected side was identified [on average, 0.173 SUVR units higher in the more affected side, 95% confidence interval (CI) = 0.11–0.24, $P < 0.0001$] (Fig. 2A). The difference in tracer retention between the more and less affected hemispheres was uniform across regions of interest (non-significant interaction between the side affected × region of interest). Regional ^{18}F-AV-1451 retention was also higher in AN-CBS subjects than in normal control subjects (for each side, $P \leqslant 0.0011$). However, there was a significant interaction of the effect of diagnostic group with region of interest ($P < 0.0001$) that *post hoc* tests showed was due to the effect of diagnostic group being especially pronounced in the precentral gyrus ($P = 0.011$) and

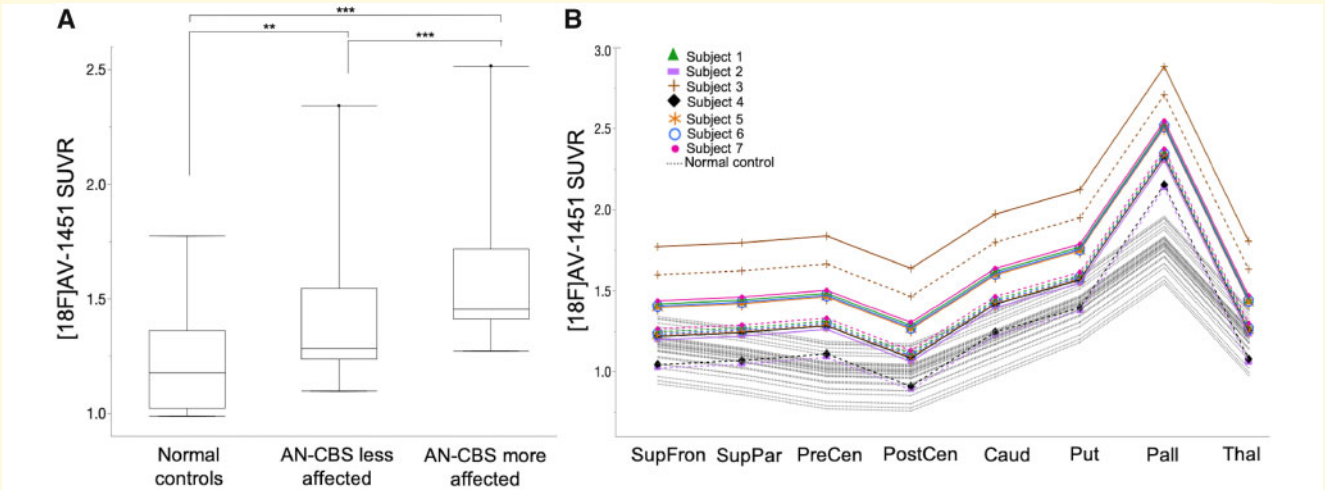

Figure 2 ^{18}F-AV-1451 retention in AN-CBS and normal control subjects. (**A**) ^{18}F-AV-1451 retention across pooled regions of interest from model-predicted means are shown for the less affected side of AN-CBS, the more affected side of AN-CBS, and normal control subjects. Box and whisker plots (median, interquartile range, minimum, maximum, and outliers) are shown. ***$P < 0.0005$, **$P < 0.005$. (**B**) ^{18}F-AV-1451 model-predicted means are shown for each region of interest for the less affected side of AN-CBS (dashed lines), the more affected side AN-CBS (solid lines), and normal control subjects (dotted lines). AN-CBS = amyloid negative cases of corticobasal syndrome (Subjects 1–7). Caud = caudate; Pall = pallidum; PostCen = postcentral; PreCen = precentral; Put = putamen; SupFron = superior frontal; SupPar = superior parietal; Thal = thalamus.

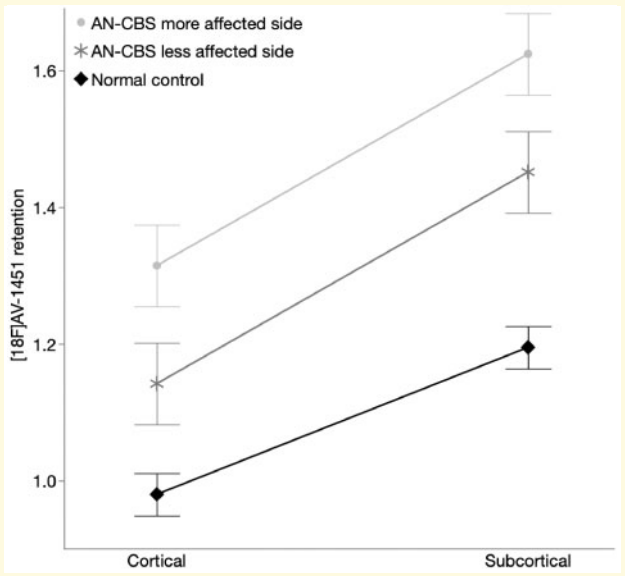

Figure 3 ^{18}F-AV-1451 retention in cortical and subcortical regions. Model-predicted means of ^{18}F-AV-1451 retention (SUVR) in cortical versus subcortical regions of interest. Note the higher retention in AN-CBS subjects' more affected side compared to their less affected side ($P < 0.0001$), the higher subcortical and cortical ^{18}F-AV-1451 retention in AN-CBS than in normal control subjects (subcortical, $P = 0.0003$; cortical, $P = 0.047$), and the steeper slope for AN-CBS subjects than for normal control subjects, reflecting a more pronounced difference between cortical and subcortical retention in AN-CBS subjects than in control subjects. Error bars reflect standard error of the model. AN-CBS = amyloid negative cases of corticobasal syndrome (Subjects 1–7).

the pallidum ($P < 0.0001$) (Fig. 2B). Together, these observations show that the pattern of ^{18}F-AV-1451 retention in AN-CBS subjects is consistent with the clinical asymmetry of disease.

To compare ^{18}F-AV-1451 retention in subcortical versus cortical regions, we used an analogous mixed effects model (see 'Materials and methods' section). In addition to the significant main effect of affected side, with higher retention in AN-CBS subjects' more affected side compared to their less affected side ($P < 0.0001$, same effect sizes as above), both subcortical and cortical ^{18}F-AV-1451 retention was greater in AN-CBS than in normal control subjects (subcortical, $P = 0.0003$; cortical, $P = 0.047$). There was also an interaction between diagnosis and subcortical/cortical region ($P = 0.014$), reflecting a finding in which there was greater retention in subcortical regions than in cortical regions in both AN-CBS and normal control subjects, but this difference was more pronounced for the AN-CBS subjects (as evidenced by the steeper slope for AN-CBS subjects than for normal control subjects in Fig. 3; $P < 0.0001$ for both AN-CBS and normal controls). These findings show that despite higher ^{18}F-AV-1451 retention in subcortical than cortical regions in normal control, ^{18}F-AV-1451 retention in AN-CBS was higher still, consistent with the underlying disease process.

Non-partial volume corrected results

To confirm that the use of PVC did not underlie these results, we applied the same analyses evaluating asymmetry of ^{18}F-AV-1451 retention and the relationship between asymmetry of ^{18}F-AV-1451 retention and asymmetry of motor function to non-PVC data. Results were broadly similar to those found with the PVC data. The ANOVAs for non-PVC ^{18}F-AV-1451 retention in AN-CBS and normal control subjects again identified a significant interaction between region of interest and diagnostic group ($P = 0.0008$). In contrast to the PVC results above, however, the interaction was strongly disordinal, i.e. it reflected variation in both the magnitude and the direction of the differences between AN-CBS and normal controls, and as a result there was no overall main effect of diagnosis. The asymmetry of ^{18}F-AV-1451 retention was greater in AN-CBS than in normal control subjects in the precentral gyrus (Tukey-adjusted $P = 0.008$) and the superior parietal gyrus (Tukey-adjusted $P = 0.036$). Diagnostic group differences were not significant in the other regions of interest.

In mixed effects general linear models to evaluate the relationship between the retention pattern of ^{18}F-AV-1451 and asymmetric motor features, there was again a significant main effect of higher ^{18}F-AV-1451 retention in AN-CBS subjects' more affected side than in the less affected side ($P = 0.0049$). Retention was also significantly higher in AN-CBS subjects compared to normal control subjects (for each side, $P \leqslant 0.045$). There was again a significant interaction of the effect of diagnostic group with region of interest ($P < 0.0001$) that *post hoc* tests in this case showed as being especially pronounced in the pallidum ($P < 0.0001$) and putamen ($P = 0.045$). There was also an interaction between diagnosis and subcortical/cortical region ($P = 0.0001$), again reflecting a finding in which there was greater retention in AN-CBS in subcortical regions than in cortical regions. Together, these results show that the asymmetric retention of ^{18}F-AV-1451 and its relation to asymmetric motor features can be detected without PVC.

Regional atrophy

Consistent with the asymmetric clinical features of both the neuropathologically proven CBD cases and the AN-CBS subjects more broadly, asymmetric cortical atrophy was evident (Fig. 1A), with visually prominent thinning of the precentral gyrus in particular. To compare the magnitude of regional asymmetric atrophy across diagnostic groups, we used the same mixed-between and within-subject factorial ANOVA as for the ^{18}F-AV-1451 measures above. These analyses showed a weakly significant interaction between region of interest and diagnostic group ($P = 0.024$), with greater asymmetry in AN-CBS in all regions of interest except the caudate (main effect of diagnosis, $P < 0.0003$). The asymmetry of atrophy trended towards being significantly greater in AN-CBS than in normal control subjects in superior parietal cortex (Tukey adjusted $P = 0.07$) and was

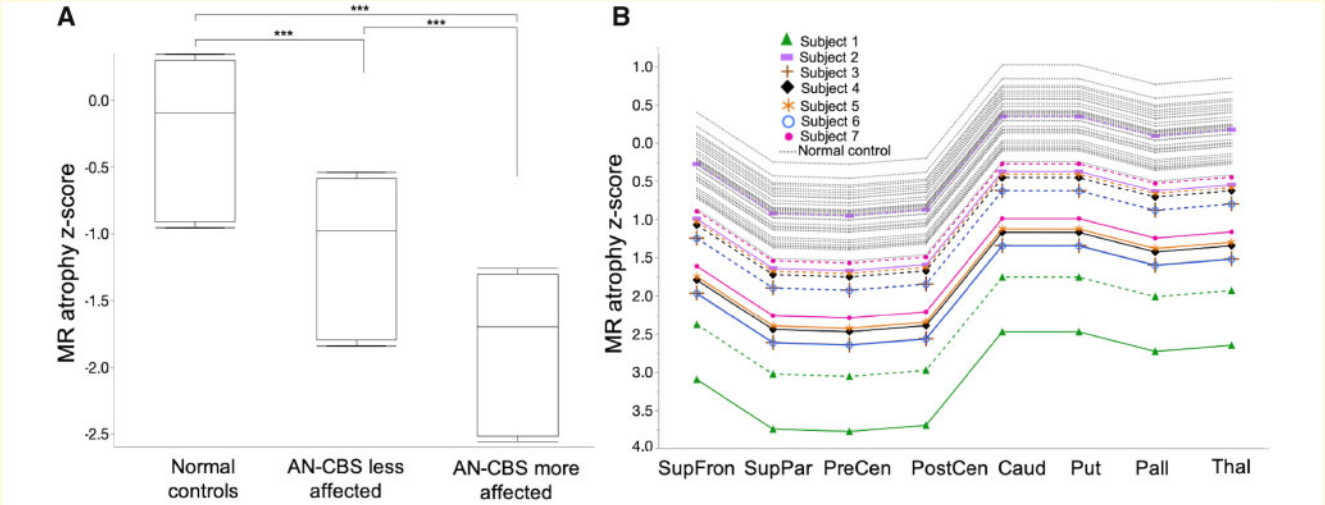

Figure 4 Atrophy in AN-CBS versus normal control subjects. (**A**) Mean atrophy across pooled regions of interest from model-predicted means is shown for the less affected side of AN-CBS, the more affected side of AN-CBS, and normal control subjects. Box and whisker plots (median, interquartile range, minimum, and maximum) are shown. *** $P < 0.0005$. (**B**) Model-predicted mean atrophy z-scores are shown for each region of interest for the less affected side of AN-CBS (dashed lines), the more affected side AN-CBS (solid lines), and normal control subjects (dotted lines). AN-CBS = amyloid negative cases of corticobasal syndrome (Subjects 1–7). Caud = caudate; Pall = pallidum; PostCen = postcentral; PreCen = precentral; Put = putamen; SupFron = superior frontal; SupPar = superior parietal; Thal = thalamus.

otherwise non-significantly different between the diagnostic groups across other regions of interest.

To quantify and compare structural changes measured with MRI in AN-CBS subjects and normal control subjects, we used a mixed effects model, as above. The mixed effects model for regional atrophy revealed a significant main effect for atrophy within and across diagnostic groups. In AN-CBS subjects, regional volume loss was greater on the more affected side (on average, the more affected side was 0.719 units lower, 95% CI 0.35–1.08, $P = 0.0001$; Fig. 4A). In addition, regional volume loss was greater in AN-CBS subjects compared to normal control subjects (on average, AN-CBS subjects' less affected sides had volumes 0.887 units lower than normal control subjects, 95% CI 0.4–1.35, $P = 0.0004$). The difference in regional atrophy measurements between AN-CBS subjects' more and less affected sides was uniform across regions of interest (non-significant interaction between the side affected × region of interest; Fig. 4B). Similarly, the difference in regional atrophy measurements between AN-CBS subjects and normal control subjects was uniform across regions of interest (non-significant interaction between diagnostic group × region of interest). Thus, in AN-CBS subjects, as with the pattern of ^{18}F-AV-1451 retention, asymmetric cortical atrophy reflected asymmetry of clinical features.

Discussion

The results of this study demonstrate moderately elevated, markedly asymmetric ^{18}F-AV-1451 retention in cortex and basal ganglia in both neuropathologically-proven CBD and AN-CBS, in concert with asymmetric cortical and subcortical atrophy, consistent with the asymmetric clinical features of CBD. In line with the high affinity of ^{18}F-AV-1451 for the paired helical filaments composed of 3R/4R tau that are observed in Alzheimer's disease, ^{18}F-AV-1451 retention was substantially higher in subjects with positive Alzheimer's disease biomarkers, as shown previously (Marquie *et al.*, 2015; Johnson *et al.*, 2016; Lowe *et al.*, 2016; Sander *et al.*, 2016). In these amyloid-positive cases, cortical ^{18}F-AV-1451 retention was also much more widely distributed than in the CBD or AN-CBS cases, in a pattern consistent with Alzheimer's disease (Johnson *et al.*, 2016). In contrast, in a CBS case proven to lack tau neuropathological changes that characterize diseases such as CBD or Alzheimer's disease, ^{18}F-AV-1451 retention was low and symmetric in cortex and basal ganglia, and cortical retention was spatially dissociated from regional cortical atrophy. Elevated retention in the thalamus and less robustly in perithalamic and frontal subcortical white matter in this tau-negative CBS case confirms the lack of specificity of ^{18}F-AV-1451 for 4R tau pathology (Marquie *et al.*, 2015; Lowe *et al.*, 2016; Sander *et al.*, 2016; Makaretz *et al.*, 2018). Although the capacity for ^{18}F-AV-1451 binding to the admixture of tau filaments present in CBD remains an open question, these findings suggest that asymmetric ^{18}F-AV-1451 retention in the cortical grey and basal ganglia is greater in patients with CBS due to CBD than in healthy subjects, raising the possibility of its clinical utility in this context.

The pattern and extent of ^{18}F-AV-1451 PET in CBD are consistent with reports of ^{18}F-AV-1451 PET in PSP, another 4R-tauopathy, in which a similar degree of modest (but more symmetric) retention has been observed in specific

brain regions susceptible to PSP pathological changes (Schonhaut *et al.*, 2017; Whitwell, 2018). The heterogeneity of tau filament structures in CBD, including numerous straight filaments and less common paired helical filaments (Tatsumi *et al.*, 2014), may also contribute. Despite this, ^{18}F-AV-1451 has not demonstrated substantial binding in CBD or PSP brain tissue (Marquie *et al.*, 2015; Lowe *et al.*, 2016; Sander *et al.*, 2016). The basis for this disparity remains unclear. Weak binding of ^{18}F-AV-1451 to the tau species in CBD that may be displaced or disrupted by tissue preparation techniques used in histological studies is possible, as is binding to an as-yet unidentified, non-tau marker of neurodegeneration that may accompany CBD and other neurodegenerative pathologies such as monoamine oxidase A (MAOA) and/or MAOB (Marquie *et al.*, 2015; Lowe *et al.*, 2016; Passamonti *et al.*, 2017; Vermeiren *et al.*, 2018), possibly related to gliosis. It is also feasible that regionally increased ^{18}F-AV-1451 retention could reflect delayed delivery or prolonged clearance of the tracer, which may be altered in areas of neurodegeneration; however, the lack of asymmetrically increased ^{18}F-AV-1451 retention in the cortex and basal ganglia of the CBS case lacking tauopathy provides some evidence against this possibility. Finally, it is possible that ^{18}F-AV-1451 may bind to small amounts of PHF tau which, although more characteristic of Alzheimer's tau pathology, have been identified in neuronal inclusions in CBD (Tatsumi *et al.*, 2014). Although the molecular basis for ^{18}F-AV-1451 retention in CBD remains to be determined, and its specificity for 4R tau is uncertain, the moderate retention in neuropathologically affected regions in both CBD and PSP suggests that ^{18}F-AV-1451 retention may be biologically meaningful.

In support of the possibility that ^{18}F-AV-1451 retention carries clinical significance in CBS, the clinically more affected hemispheres of AN-CBS subjects demonstrated greater ^{18}F-AV-1451 retention and greater atrophy, consistent with a recent report (Niccolini *et al.*, 2018). Furthermore, both ^{18}F-AV-1451 retention and atrophy—and the magnitude of asymmetry of ^{18}F-AV-1451 retention and atrophy—were greater in AN-CBS subjects compared to normal control subjects, as shown previously (Cho *et al.*, 2017; Smith *et al.*, 2017; Niccolini *et al.*, 2018). We also found greater retention of ^{18}F-AV-1451 in subcortical regions compared to the cortical regions assessed. Although off-target ^{18}F-AV-1451 retention in the basal ganglia has been described in some healthy subjects (Passamonti *et al.*, 2017), the greater subcortical retention in our cohort of AN-CBS subjects compared to normal control subjects implicates a distinct process related to the underlying pathology. Together, these findings suggest that ^{18}F-AV-1451 retention in AN-CBS, as in autopsy-proven cases of CBD, reflects the asymmetric neurodegenerative process associated with the clinical manifestations that characterize CBS due to CBD. Our results additionally support the added value of molecular neuroimaging with ^{18}F-AV-1451 over MRI alone in distinguishing CBS due to underlying Alzheimer's disease pathology from other aetiologies of CBS. Although amyloid-PET may also be useful for this purpose, tau-PET bypasses the risk of incidental amyloid positivity in patients with primary CBD and may provide a more definitive link to the aetiology of CBS in Alzheimer's disease.

Strengths of this study include the evaluation of clinically well-characterized participants with CBS, as well as neuropathological confirmation in six cases. Despite the limited sample size, which is typical in studies of uncommon diseases such as CBD, the use of mixed effects models allowed us to make sensitive contrasts across diagnostic groups, hemispheres, and regions of interest that were robust to presence or absence of PVC. A potential limitation of this study is the relatively long interval between PET acquisition and autopsy in some subjects, which could in principle have contributed to mismatch between PET and neuropathological findings. Another limitation is the lack of subjects with additional autopsy-proven pathologies that can be seen in CBS such as FTLD-TDP43 or prion disease. Additional research will be required to examine ^{18}F-AV-1451 retention in such cases. Additionally, although radiographic-pathological correlation was not possible in all subjects, we will continue to collect autopsy data as they become available. We conclude that ^{18}F-AV-1451 retention in CBD captures the pattern of underlying tau burden, even though it appears to underestimate its magnitude. These findings set the stage for future quantitative ^{18}F-AV-1451 PET—neuropathological correlations and larger studies needed to determine whether ^{18}F-AV-1451 will have utility for the antemortem diagnosis of CBD.

Acknowledgements

We thank the radiopharmacy and imaging staff at the Gordon Center for Medical Imaging and the Athinoula A. Martinos Center for Biomedical Imaging, as well as the subjects and their families.

Funding

This work was supported by NIH 1 R21 NS 090243–01 (S.G.), ROI AG046396 (K.J.), R01 DC014296 (B.C.D.), and P30 AG062421 and was carried out in part at the Athinoula A. Martinos Center for Biomedical Imaging at Massachusetts General Hospital, using resources provided by the Center for Functional Neuroimaging Technologies, P41EB015896, a P41 Biotechnology Resource Grant supported by the National Institute of Biomedical Imaging and Bioengineering (NIBIB), National Institutes of Health. This work also involved use of instrumentation supported by the NIH Shared Instrumentation Grant Program and/or High-End Instrumentation Grant Program; specifically, grant numbers S10RR023401, S10RR023043, S10RR021110.

Competing interests

A.E.G., J.J.L., W.R.S., J.A.C., M.B., A.S., A.T. report no competing interests. K.A.J. has served as a paid consultant for Bayer, GE Healthcare, Janssen Alzheimer's Immunotherapy, Siemens Medical Solutions, Genzyme, Novartis, Biogen, Roche, ISIS Pharma, AZTherapy, GEHC, Lundberg, and Abbvie. He is a site coinvestigator for Lilly/Avid, Pfizer, Janssen Immunotherapy, and Navidea. He has spoken at symposia sponsored by Janssen Alzheimer's Immunotherapy and Pfizer. He receives funding from NIH grants R01EB014894, R21 AG038994, R01 AG026484, R01 AG034556, P50 AG00513421, U19 AG10483, P01 AG036694, R13 AG042201174210, R01 AG027435, and R01 AG037497 and the Alzheimer's Association grant ZEN-10-174210. M.P.F. receives funding support from NIH, serves on external advisory committees for University of Michigan and Norwestern Feinberg School of Medicine, and serves as the PI for Sponsored Research Agreements between Massachusetts General Hospital with Biogen and Voyager Therapeutics. J.G. reports support from NIA and Advisory Board Neuroimmune Holding. B.C.D. has served as a paid consultant for Novartis, Avexis, Biogen, Lilly, Wave LifeSciences, Merck, and Arkuda. He receives royalties from Oxford University Press and Cambridge University Press. He receives funding from NIH grants P01 AG036694, R01 AG045390, R01 AG038791, R01 AG048351, R01 DC014296, U01 AG052943, R01 AG056015, R21 AG056958, R01 AG054081, R01MH112737, R01MH109464, R01MH113234, R56AG058745, U01AG057195, R01 AG0061968, P01 AG031720, P30AG062421, R01DC014296, the Alzheimer's Drug Discovery Foundation and the ALS Association. S.N.G. has served on Advisory Boards for Acadia Pharmaceuticals and Sanofi. He receives funding from NIH grant R01 AG054551, R01 AG062208, P50 AG005134, R21 NS109833, P30AG062421, DOD CDMRP/W81XW1810516, the Farmer Family Parkinson's Initiative, and the Lewy Body Dementia Association.

Supplementary material

Supplementary material is available at *Brain* online.

References

Ali F, Whitwell JL, Martin PR, Senjem ML, Knopman DS, Jack CR, et al. [(18)F] AV-1451 uptake in corticobasal syndrome: the influence of beta-amyloid and clinical presentation. J Neurol 2018; 265: 1079–88.

Armstrong MJ, Litvan I, Lang AE, Bak TH, Bhatia KP, Borroni B, et al. Criteria for the diagnosis of corticobasal degeneration. Neurology 2013; 80: 496–503.

Arnold SE, Toledo JB, Appleby DH, Xie SX, Wang LS, Baek Y, et al. Comparative survey of the topographical distribution of signature molecular lesions in major neurodegenerative diseases. J Comp Neurol 2013; 521: 4339–55.

Bakkour A, Morris JC, Dickerson BC. The cortical signature of prodromal AD: regional thinning predicts mild AD dementia. Neurology 2009; 72: 1048–55.

Boeve BF, Maraganore DM, Parisi JE, Ahlskog JE, Graff-Radford N, Caselli RJ, et al. Pathologic heterogeneity in clinically diagnosed corticobasal degeneration. Neurology 1999; 53: 795–800.

Braak H, Braak E. Neuropathological stageing of Alzheimer-related changes. Acta Neuropathol 1991; 82: 239–59.

Cairns NJ, Bigio EH, Mackenzie IR, Neumann M, Lee VM, Hatanpaa KJ, et al. Neuropathologic diagnostic and nosologic criteria for frontotemporal lobar degeneration: consensus of the Consortium for Frontotemporal Lobar Degeneration. Acta Neuropathol 2007; 114: 5–22.

Chien DT, Bahri S, Szardenings AK, Walsh JC, Mu F, Su MY, et al. Early clinical PET imaging results with the novel PHF-tau radioligand [F-18]-T807. J Alzheimers Dis 2013; 34: 457–68.

Cho H, Baek MS, Choi JY, Lee SH, Kim JS, Ryu YH, et al. (18)F-AV-1451 binds to motor-related subcortical gray and white matter in corticobasal syndrome. Neurology 2017; 89: 1170–8.

Coakeley S, Ang LC, Jansen GH, Cho SS, Lang AE, Houle S, et al. [18 F]AV-1451 binding and postmortem pathology of CBD. Mov Disord 2018; 33: 1360–1.

Dickerson BC, Bakkour A, Salat DH, Feczko E, Pacheco J, Greve DN, et al. The cortical signature of Alzheimer's disease: regionally specific cortical thinning relates to symptom severity in very mild to mild AD dementia and is detectable in asymptomatic amyloid-positive individuals. Cereb Cortex 2009; 19: 497–510.

Dickson DW, Bergeron C, Chin SS, Duyckaerts C, Horoupian D, Ikeda K, et al. Office of rare diseases neuropathologic criteria for corticobasal degeneration. J Neuropathol Exp Neurol 2002; 61: 935–46.

Fischl B, Dale AM. Measuring the thickness of the human cerebral cortex from magnetic resonance images. Proc Natl Acad Sci USA 2000; 97: 11050–5.

Fischl B, van der Kouwe A, Destrieux C, Halgren E, Segonne F, Salat DH, et al. Automatically parcellating the human cerebral cortex. Cereb Cortex 2004; 14: 11–22.

Folstein MF, Folstein SE, McHugh PR. "Mini-mental state". A practical method for grading the cognitive state of patients for the clinician. J Psychiatr Res 1975; 12: 189–98.

Goetz CG, Fahn S, Martinez-Martin P, Poewe W, Sampaio C, Stebbins GT, et al. Movement Disorder Society-sponsored revision of the Unified Parkinson's Disease Rating Scale (MDS-UPDRS): Process, format, and clinimetric testing plan. Mov Disord 2007; 22: 41–7.

Goetz CG, Tilley BC, Shaftman SR, Stebbins GT, Fahn S, Martinez-Martin P, et al. Movement Disorder Society-sponsored revision of the Unified Parkinson's Disease Rating Scale (MDS-UPDRS): scale presentation and clinimetric testing results. Mov Disord 2008; 23: 2129–70.

Greve DN, Salat DH, Bowen SL, Izquierdo-Garcia D, Schultz AP, Catana C, et al. Different partial volume correction methods lead to different conclusions: an (18)F-FDG-PET study of aging. Neuroimage 2016; 132: 334–43.

Hoglinger GU, Respondek G, Stamelou M, Kurz C, Josephs KA, Lang AE, et al. Clinical diagnosis of progressive supranuclear palsy: the movement disorder society criteria. Mov Disord 2017; 32: 853–64.

Hyman BT, Phelps CH, Beach TG, Bigio EH, Cairns NJ, Carrillo MC, et al. National Institute on Aging-Alzheimer's Association guidelines for the neuropathologic assessment of Alzheimer's disease. Alzheimers Dement 2012; 8: 1–13.

Jabbari E, Holland N, Chelban V, Jones PS, Lamb R, Rawlinson C, et al. Diagnosis across the spectrum of progressive supranuclear palsy and corticobasal syndrome. JAMA Neurol 2019; 77: 377–87.

Johnson KA, Schultz A, Betensky RA, Becker JA, Sepulcre J, Rentz D, et al. Tau positron emission tomographic imaging in aging and early Alzheimer disease. Ann Neurol 2016; 79: 110–9.

Josephs KA, Whitwell JL, Tacik P, Duffy JR, Senjem ML, Tosakulwong N, et al. [18F]AV-1451 tau-PET uptake does

correlate with quantitatively measured 4R-tau burden in autopsy-confirmed corticobasal degeneration. Acta Neuropathol 2016; 132: 931–3.

Klunk WE, Engler H, Nordberg A, Wang Y, Blomqvist G, Holt DP, et al. Imaging brain amyloid in Alzheimer's disease with Pittsburgh Compound-B. Ann Neurol 2004; 55: 306–19.

Lee SE, Rabinovici GD, Mayo MC, Wilson SM, Seeley WW, DeArmond SJ, et al. Clinicopathological correlations in corticobasal degeneration. Ann Neurol 2011; 70: 327–40.

Ling H, O'Sullivan SS, Holton JL, Revesz T, Massey LA, Williams DR, et al. Does corticobasal degeneration exist? A clinicopathological re-evaluation. Brain 2010; 133: 2045–57.

Logan J, Fowler JS, Volkow ND, Wang GJ, Ding YS, Alexoff DL. Distribution volume ratios without blood sampling from graphical analysis of PET data. J Cereb Blood Flow Metab 1996; 16: 834–40.

Lowe VJ, Curran G, Fang P, Liesinger AM, Josephs KA, Parisi JE, et al. An autoradiographic evaluation of AV-1451 Tau PET in dementia. Acta Neuropathol Commun 2016; 4: 58.

Makaretz SJ, Quimby M, Collins J, Makris N, McGinnis S, Schultz A, et al. Flortaucipir tau PET imaging in semantic variant primary progressive aphasia. J Neurol Neurosurg Psychiatry 2018; 89: 1024–31.

Marquie M, Normandin MD, Vanderburg CR, Costantino IM, Bien EA, Rycyna LG, et al. Validating novel tau positron emission tomography tracer [F-18]-AV-1451 (T807) on postmortem brain tissue. Ann Neurol 2015; 78: 787–800.

Mathis CA, Wang Y, Holt DP, Huang GF, Debnath ML, Klunk WE. Synthesis and evaluation of 11C-labeled 6-substituted 2-arylbenzothiazoles as amyloid imaging agents. J Med Chem 2003; 46: 2740–54.

McMillan CT, Irwin DJ, Nasrallah I, Phillips JS, Spindler M, Rascovsky K, et al. Multimodal evaluation demonstrates in vivo (18)F-AV-1451 uptake in autopsy-confirmed corticobasal degeneration. Acta Neuropathol 2016; 132: 935–7.

Mirra SS, Heyman A, McKeel D, Sumi SM, Crain BJ, Brownlee LM, et al. The consortium to establish a registry for Alzheimer's Disease (CERAD). Part II. Standardization of the neuropathologic assessment of Alzheimer's disease. Neurology 1991; 41: 479–86.

Morris JC. Clinical dementia rating: a reliable and valid diagnostic and staging measure for dementia of the Alzheimer type. Int Psychogeriatr 1997; 9 (Suppl 1): 173–6. discussion 7–8.

Nasreddine ZS, Phillips NA, Bedirian V, Charbonneau S, Whitehead V, Collin I, et al. The Montreal Cognitive Assessment, MoCA: a brief screening tool for mild cognitive impairment. J Am Geriatr Soc 2005; 53: 695–9.

Niccolini F, Wilson H, Hirschbichler S, Yousaf T, Pagano G, Whittington A, et al. Disease-related patterns of in vivo pathology in Corticobasal syndrome. Eur J Nucl Med Mol Imaging 2018; 45: 2413–25.

Ono M, Sahara N, Kumata K, Ji B, Ni R, Koga S, et al. Distinct binding of PET ligands PBB3 and AV-1451 to tau fibril strains in neurodegenerative tauopathies. Brain 2017; 140: 764–80.

Passamonti L, Vazquez Rodriguez P, Hong YT, Allinson KS, Williamson D, Borchert RJ, et al. 18F-AV-1451 positron emission tomography in Alzheimer's disease and progressive supranuclear palsy. Brain 2017; 140: 781–91.

Rebeiz JJ, Kolodny EH, Richardson EP. Jr., Corticodentatonigral degeneration with neuronal achromasia: a progressive disorder of late adult life. Trans Am Neurol Assoc 1967; 92: 23–6.

Sander K, Lashley T, Gami P, Gendron T, Lythgoe MF, Rohrer JD, et al. Characterization of tau positron emission tomography tracer [(18)F]AV-1451 binding to postmortem tissue in Alzheimer's disease, primary tauopathies, and other dementias. Alzheimers Dement 2016; 12: 1116–24.

Schonhaut DR, McMillan CT, Spina S, Dickerson BC, Siderowf A, Devous MD Sr, et al. (18) F-flortaucipir tau positron emission tomography distinguishes established progressive supranuclear palsy from controls and Parkinson disease: a multicenter study. Ann Neurol 2017; 82: 622–34.

Shoup TM, Yokell DL, Rice PA, Jackson RN, Livni E, Johnson KA, et al. A concise radiosynthesis of the tau radiopharmaceutical, [(18)F]T807. J Label Compd Radiopharm 2013; 56: 736–40.

Smith R, Scholl M, Widner H, van Westen D, Svenningsson P, Hagerstrom D, et al. In vivo retention of (18)F-AV-1451 in corticobasal syndrome. Neurology 2017; 89: 845–53.

Tatsumi S, Uchihara T, Aiba I, Iwasaki Y, Mimuro M, Takahashi R, et al. Ultrastructural differences in pretangles between Alzheimer disease and corticobasal degeneration revealed by comparative light and electron microscopy. Acta Neuropathol Commun 2014; 2: 161.

Tsai RM, Bejanin A, Lesman-Segev O, LaJoie R, Visani A, Bourakova V, et al. F-flortaucipir (AV-1451) tau PET in frontotemporal dementia syndromes. Alzheimers Res Ther 2019; 11:13.

Upadhyay N, Suppa A, Piattella MC, Di Stasio F, Petsas N, Colonnese C, et al. Gray and white matter structural changes in corticobasal syndrome. Neurobiol Aging 2016; 37: 82–90.

Vermeiren C, Motte P, Viot D, Mairet-Coello G, Courade JP, Citron M, et al. The tau positron-emission tomography tracer AV-1451 binds with similar affinities to tau fibrils and monoamine oxidases. Mov Disord 2018; 33: 273–81.

Villemagne VL, Fodero-Tavoletti MT, Masters CL, Rowe CC. Tau imaging: early progress and future directions. Lancet Neurol 2015; 14: 114–24.

Vonsattel JP, Del Amaya MP, Keller CE. Twenty-first century brain banking. Processing brains for research: the Columbia University methods. Acta Neuropathol 2008; 115: 509–32.

Walker Z, Gandolfo F, Orini S, Garibotto V, Agosta F, Arbizu J, et al. Clinical utility of FDG PET in Parkinson's disease and atypical parkinsonism associated with dementia. Eur J Nucl Med Mol Imaging 2018; 45: 1534–45.

Weintraub S, Salmon D, Mercaldo N, Ferris S, Graff-Radford NR, Chui H, et al. The Alzheimer's Disease Centers' Uniform Data Set (UDS): the neuropsychologic test battery. Alzheimer Dis Assoc Disord 2009; 23: 91–101.

Whitwell JL. Tau Imaging in Parkinsonism: what Have We Learned So Far? Mov Disord Clin Pract 2018; 5: 118–30.

Xia C, Makaretz SJ, Caso C, McGinnis S, Gomperts SN, Sepulcre J, et al. Association of in vivo [18F]AV-1451 Tau PET imaging results with cortical atrophy and symptoms in typical and atypical Alzheimer Disease. JAMA Neurol 2017; 74: 427–36.

Xia CF, Arteaga J, Chen G, Gangadharmath U, Gomez LF, Kasi D, et al. [(18)F]T807, a novel tau positron emission tomography imaging agent for Alzheimer's disease. Alzheimers Dement 2013; 9: 666–76.